IEEE Open Journal of
Industry Applications

Received 8 February 2022; revised 11 April 2022; accepted 26 April 2022. Date of publication 29 April 2022;
date of current version 18 May 2022. The review of this article was arranged by Associate Editor Mauro Di Nardo.

Digital Object Identifier 10.1109/OJIA.2022.3171333

Data-Driven Adaptive Torque Oscillation Compensation for Multi-Motor Drive Systems

ANIAN BROSCH [1], JOHANN RAUHAUS [2], OLIVER WALLSCHEID [1] (Member, IEEE), DETMAR ZIMMER [2], AND JOACHIM BÖCKER [1] (Senior Member, IEEE)

[1]Department of Power Electronics and Electrical Drives, Paderborn University, 33098 Paderborn, Germany
[2]Chair of Design and Drive Technology (KAt), Paderborn University, 33098 Paderborn, Germany

CORRESPONDING AUTHOR: ANIAN BROSCH (e-mail: anian.brosch@uni-paderborn.de)

This work was supported by the German Research Foundation (DFG) under Grant 389029890.

ABSTRACT Multi-motor drive systems (MMDS) combine several drives that work together to fulfill one task. Compared to conventional single-motor drive systems modular product concepts can be realized with MMDS thanks to additional degrees of freedom. Because of their mechanical structure consisting of several shafts, clutches, and gear pairings, complex deflection shapes arise which lead to unintended torque oscillations.To compensate for these torque oscillations a data-driven adaptive multiple-input single-output scheme based on two cascaded recursive least squares estimators is proposed. Here, weights (manipulable amplitudes) for each order (multiple of a fundamental frequency) to be compensated are multiplied with unit amplitude harmonic signals of a reference oscillator and added as reference torques to the torque controllers of the MMDS's drives. These weights are continually adapted by an online identification of transfer paths and disturbances. Furthermore, the torque contribution of the individual drives concerning the compensation task can be changed at runtime utilizing a weighting matrix as tuning parameter by analytically solving a quadratic program with a linear equality constraint. Hence, the proposed algorithm is suitable for automatic self-commissioning requiring only marginal expert intervention. Experimental investigations prove the compensation capability of the approach whereby a reduction of the output torque's total harmonic distortion (THD) of up to 80% from 26.8% to 5.4% for a representative operation point is achieved.

INDEX TERMS Disturbance compensation, harmonic steady state, identification, multi-motor drive system, recursive least squares, torque oscillation.

NOMENCLATURE

$m \in \mathbb{N}$	number of electric motors of the MMDS
$r \in \mathbb{N}$	number of orders that should be compensated
$p_i \in \mathbb{R}$	value of i-th order
$k \in \mathbb{N}$	time index of the overall compensation scheme
$n \in \mathbb{N}$	time index of the adaptive compensators
$\underline{x} \in \mathbb{C}$	complex scalar
$\boldsymbol{x} \in \mathbb{R}^v$	real vector
$\boldsymbol{X} \in \mathbb{R}^{f \times g}$	real matrix
$\underline{x}^*$	complex conjugate of $\underline{x}$
$\boldsymbol{x}^{\mathrm{T}}$	transpose of $\boldsymbol{x}$
$\underline{\boldsymbol{x}}^{\mathrm{H}}$	complex conjugate transpose of $\underline{\boldsymbol{x}}$

I. INTRODUCTION

While more and more application-specific and customized products are being developed, manufacturers in the drive technology sector are facing increased cost pressure due to highly-globalized markets and shakeouts consolidating the market. Modular product concepts based on standardized components can help to handle the manufacturer's product complexity and cost structure [1]–[3]. Here, multi-motor drive systems (MMDS) [4]–[9] can be a promising alternative compared to single-motor drive systems (SMDS) thanks to a higher amount of standardized cross-over parts, see Fig. 1. Furthermore if a fault occurs within an SMDS component,

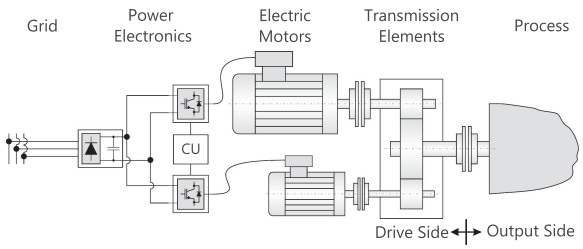

FIG. 1. General structure of an MMDS (derivate of [3]).

this situation inevitably leads to a massive impairment of the functionality or even a total shutdown of the SMDS. By distributing the rated power over several motors, the MMDS can continue to operate at reduced power or at least be shut down in a safe way in the case of a motor or converter fault. As a result, an MMDS has an inherent fail operational capability and, thus, improved availability compared to an SMDS. Moreover, for drive applications with variable output power, frequently changing operating points and many partial load situations, a reduced average efficiency of an SMDS compared to its rated conditions must be accepted [3], [10]. Here, the efficiency at partial load can be increased by utilizing an MMDS, where only the minimum number of motors is involved to provide the currently demanded drive power and the motors that are temporarily not needed are mechanically and electrically decoupled [3].

Due to the increased number of mechanical components in the MMDS, however, disadvantages arise as well. Because of the MMDS's mechanical structure different phenomena are the root cause of significant unintended mechanical oscillations. These are, e.g., tooth meshing, static and dynamic mechanical imbalances due to variations in the manufacturing process, misalignment of rotor shafts, mechanical backlash, and higher harmonics in the electromagnetic torque produced by the electric motors due to a nonsinusoidal flux distribution in the air gap. These phenomena are generally frequency-dependent and can be interpreted as harmonic disturbances. Often the frequencies of these harmonic disturbances are multiples of the rotational speed of the MMDS. These multiples are often integers but can also be fractional, e.g. due to a fractional gear ratio. If the frequency of a harmonic disturbance coincides with a resonance frequency of the weakly damped mechanical structure of an MMDS, significant mechanical oscillations can occur. These mechanical vibrations must be avoided as they excite the connected process via the output shaft, leading to additional wear and tear as well as to unwanted noise radiation.

A. STATE-OF-THE-ART TECHNIQUES

Vibration damping of mechanical structures can be classified into two areas. One is passive damping of the structure by adding viscoelastic materials, viscous fluids, magnetics, or passive piezoelectrics to dissipate energy [11]–[13]. The other one is active damping by rejecting the harmonic disturbances with the help of an actuator and a closed-loop control [14]–[16]. Since actuators are inherently included in an MMDS, namely the electrical drives, which can damp or cancel harmonic torque vibrations on the output shaft, active damping methods are the economic choice.

Harmonic disturbance rejection is of significant interest in the field of control engineering and a well established research topic. For this reason numerous examples show the successful use of a variety of methods that can be assigned to active damping by harmonic disturbance rejection. These include the application within mechatronic single-input single-ouput (SISO) systems, e.g., SMDSs [16]–[19], disk drives [20]–[22], gearboxes [23]–[25], and furthermore the control of power electronic devices [26], [27] or industrial processes [28]–[31].

A widely used method for narrow and broadband disturbance compensation is the Filtered-x-LMS (Fx-LMS) algorithm [32]–[34], which is an extension of the least mean squares (LMS) adaptive filter algorithm [35]. Here, the disturbance must be measured and the transfer path from the actuator to the sensor of the output measurement must be known.

If the harmonic disturbance is not measured but its frequency is known, the internal model principle (IMP) can be applied for compensation [36]–[38]. This is based on the assumption that the harmonic disturbance can be represented as the output of a known disturbance model with an unknown internal disturbance state. If an output feedback control loop is used, a controller with an internal dynamic must be utilized that contains the dynamic of the disturbance model. Another IMP approach is the usage of a disturbance observer to estimate the disturbance state and apply a disturbance state feedback. If the frequency of the disturbance changes, which is the case for an MMDS, the dynamic controller or disturbance observer must be reconfigured leading to additional computational load.

So-called harmonic steady-state (HSS) methods are another group of harmonic disturbance rejection methods [23], [31], [39]–[42]. All HSS algorithms have in common that they assume a steady state of oscillation, which simplifies the compensation problem, since the response of the system to a known sinusoidal excitation is characterized by only one complex scalar value, namely the value of the plant's transfer function at the particular excitation frequency. Other HSS methods exist that adapt to a changing plant transfer function by measuring the plant's output, such that an a priori offline system identification is not necessary [23], [39], [40], [42]. Since HSS methods approximate the plant via its steady-state sinusoidal response, HSS algorithms can be classified as very computationally efficient during online operation.

B. CHALLENGES OF MMDS TORQUE OSCILLATION COMPENSATION

For model-based torque compensation of an MMDS a state-space model that represents the mechanical and electrical behavior of the MMDS with sufficient accuracy is required. Determining this model is complicated for the following reasons:

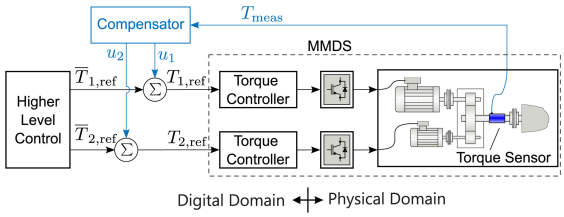

FIG. 2. Control structure of an MMDS for $m = 2$ motors with the proposed compensator scheme (blue parts are focused within this work).

1) The mechanical part of the MMDS consisting of continuously distributed masses and stiffnesses described by partial differential equations (PDE) must be approximated as a multibody system and lumped parameters with ordinary differential equations (ODE).
2) Highly nonlinear effects like nonlinear mechanical friction and backlash in gear pairings make the application of a global linear model impossible.
3) The mechanical impedance of the load must be also modeled. Here, the mechanical impedance may also be nonlinear and time variant which further complicate the modeling and identification process.
4) For reconfigurable MMDS with mechanically decoupleable drives, it is necessary to determine one model for each possible combination of coupled motors. Hence, the number of required models increases exponentially with the number of motors.

C. CONTRIBUTION

Instead of applying a model-based approach, a data-driven adaptive torque compensation method is proposed. For this reason, extensive modeling and offline system identification for parameter estimation, which is usually based on first-order physical principles and, therefore, includes systematic errors, can be avoided. The proposed approach of harmonic disturbance rejection can be classified as an HSS method for multiple-input single-output (MISO) systems with an integrated online identification of the plant transfer paths and the disturbances that lead to harmonic torque oscillations. In the case of an MMDS as MISO system, the proposed compensation scheme calculates compensation signals $\boldsymbol{u}(t)^{\mathrm{T}} = [u_1(t) \quad u_2(t) \quad \dots \quad u_m(t)]$ based on the input-output relation between the compensation signals as inputs and the scalar torque $T_{\text{meas}}(t)$ as output at the shaft of the MMDS. These compensation signals $\boldsymbol{u}(t)$ are superimposed on the mean reference torques $\overline{\boldsymbol{T}}^{\mathrm{T}}_{\text{ref}}(t) = [\overline{T}_{1,\text{ref}}(t) \quad \overline{T}_{2,\text{ref}}(t) \quad \dots \quad \overline{T}_{\text{m,ref}}(t)]$ of the torque controllers of the drives such that the unintended torque oscillations disappear to highest achievable extent, see Fig. 2. The torque T_{meas} of the shaft of the MMDS is directly measured since for the application of a torque observer instead of a direct measurement sophisticated disturbance and system models of the MMDS are required. The availability of adequate system and disturbance models for MMDS has not yet been demonstrated and is, therefore, questionable, see Section I-B. Since only the torque output of the MMDS must be measured for the proposed scheme, only one torque sensor is required. To compensate for r harmonic torque components of $T_{\text{meas}}(t)$, the harmonic reference torque signal $u_i(t)$ for the i-th of the m drive must also contain r harmonic components. This leads to a number of $r \cdot m$ amplitudes and phases characterizing $\boldsymbol{u}(t)$ that have to be calculated by the compensation scheme.

The overall compensation scheme contains the following elements:

1) Generation of sine and cosine reference signals for r predefined orders that need to be compensated by utilizing the measured rotor angle of one of the MMDS motors.
2) Estimation of harmonic torque phasors with a recursive least squares (RLS) algorithm on the basis of the sine and cosine reference signals of a).
3) One adaptive compensator for each order that continually identifies the plant's transfer paths and the disturbance with the help of complex-valued RLS (cRLS) estimators on the basis of the corresponding torque phasor of b). With the help of the estimated transfer paths and the disturbance, a weighted sum of the sine and cosine reference signals of a) is applied as compensation signal that cancels the torque oscillation. Furthermore, a weighting matrix is introduced to adjust the compensation torque distribution among the m drives of the MMDS.

Since 1) and 2) are standard procedures of HSS methods [39], 3) and the application of the overall compensation scheme on an MMDS represents the core contribution of this work.

D. PAPER STRUCTURE

This paper is organized as follows. Section II describes the overall compensation scheme. Here, the online identification of the transfer paths and disturbances as well as the distribution of the compensation task between the MMDS's drives via tuning parameters are focused. Extensive experimental investigations for a quasi-steady-state speed ramp and a changing distribution of the drives' compensation task are discussed in Section III. Finally, Section IV concludes the paper.

II. OVERALL COMPENSATION SCHEME

A. MATHEMATICAL FRAMEWORK

Assuming steady-state torque control conditions for each drive and up to r harmonic torques, the measured torque

$$\begin{aligned} T_{\text{meas}}(t) &= \overline{T}_{\text{meas}} + \sum_{i=1}^{r} e_{\text{c},i} \cos(\omega_i t) + e_{\text{s},i} \sin(\omega_i t) \\ &= \overline{T}_{\text{meas}} + \underbrace{\operatorname{Re}\left(\sum\nolimits_{i=1}^{r} \underline{e}_i \exp\left(-\mathrm{j}\omega_i t\right)\right)}_{e(t)} \end{aligned} \tag{1}$$

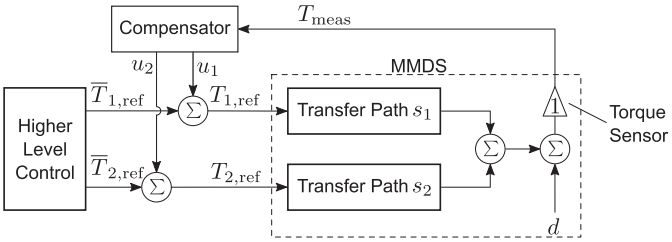

FIG. 3. Block diagram of an MMDS for $m = 2$ motors.

contains a constant component $\overline{T}_{\text{meas}}$ and a harmonic component $e(t)$ characterized by phasors $\underline{e}_i = e_{\text{c},i} + \text{j}e_{\text{s},i}$. The angular frequency of the i-th harmonic torque is given by

$$\omega_i = p_i \omega \tag{2}$$

with order number p_i and the shaft's angular velocity ω. The order numbers p_i can be simply identified with the help of a Campbell diagram and a speed ramp as described later in Section III-B, which can be implemented as an automatic self-commissioning process. In (1) sideband harmonics are assumed to be neglectable and, therefore, not represented in (2). Furthermore the torque sensor's transfer function is assumed to be ideal such that the measured torque on the output shaft of the MMDS is equal to the actual torque (cf. Fig. 3). Since the harmonic torque $e(t)$ is unintended, a reference value for the harmonic torque would be zero and, therefore, the harmonic torque $e(t)$ is referred to as a (control) error signal for the compensator in the remainder of the paper. The harmonic component $e(t)$ is caused by a superposition of harmonic disturbances $d(t)$ and the compensation signal $\boldsymbol{u}(t)$ filtered by the transfer function paths $\underline{\boldsymbol{s}}(\omega_i)^{\text{T}} = [\underline{s}_1(\omega_i) \quad \underline{s}_2(\omega_i) \quad \dots \quad \underline{s}_m(\omega_i)]$ from the reference of the conventional torque controllers to the torque sensor (cf. Figs. 2 and 3). The output signal $\boldsymbol{u}(t)$ of the compensator contains the harmonic reference torques for the m electrical drives. These superimpose the mean reference torques that are provided by a higher-level control loop. Under the assumption of linear transfer paths $\underline{\boldsymbol{s}}(\omega_i)$ the compensation signal $\boldsymbol{u}(t)$ has to be of the following form

$$\begin{aligned}\boldsymbol{u}(t) &= \sum_{i=1}^{r} \boldsymbol{w}_{\text{c},i} \cos(\omega_i t) + \boldsymbol{w}_{\text{s},i} \sin(\omega_i t) \\ &= \text{Re}\left(\sum_{i=1}^{r} \underline{\boldsymbol{w}}_i^* \exp(-\text{j}\omega_i t) \right)\end{aligned} \tag{3}$$

to compensate for harmonic disturbances with m-dimensional manipulable weight phasor vectors $\underline{\boldsymbol{w}}_i^* = \boldsymbol{w}_{\text{c},i} + \text{j}\boldsymbol{w}_{\text{s},i}$ and trigonometric signals $\cos(\omega_i t)$ and $\sin(\omega_i t)$ generated by a reference oscillator. Similar to the error signal $e(t)$ and the compensation signal $\boldsymbol{u}(t)$, the additive harmonic torque disturbance $d(t)$ can be represented in phasor notation

$$\begin{aligned}d(t) &= \sum_{i=1}^{r} d_{\text{c},i} \cos(\omega_i t) + d_{\text{s},i} \sin(\omega_i t) \\ &= \text{Re}\left(\sum_{i=1}^{r} \underline{d}_i \exp(-\text{j}\omega_i t) \right)\end{aligned} \tag{4}$$

with the disturbance phasors $\underline{d}_i = d_{\text{c},i} + \text{j}d_{\text{s},i}$. The phasors of the error, disturbance, and compensation signals are linked by the following equation for every order p_i which is fundamental for the formulation of the compensation scheme:

$$\underline{e}_i = \underline{\boldsymbol{w}}_i^{\text{H}} \underline{\boldsymbol{s}}(\omega_i) + \underline{d}_i. \tag{5}$$

For each order p_i that has to be canceled an adaptive compensator is utilized that identifies the transfer path vector $\underline{\boldsymbol{s}}_i := \underline{\boldsymbol{s}}(\omega_i)$ and the disturbance $\underline{d}_i$ online and selects the manipulable weight vector $\underline{\boldsymbol{w}}_i$ in such a way that the error signal amplitudes $\underline{e}_i$ are minimized.

The overall compensation scheme contains the following elements, which are described in more detail in the following subsections (cf. Fig. 4):

1) Generation of sine and cosine signals with unit amplitude for predefined orders p_i.
2) Estimation of the error phasors $\underline{e}_i$ with an RLS algorithm.
3) An adaptive compensator for each order p_i that continuously identifies the transfer path vectors $\underline{\boldsymbol{s}}_i$ and the disturbances $\underline{d}_i$ to choose the weight vector $\underline{\boldsymbol{w}}_i$ such that the torque oscillation $\underline{e}_i$ of the corresponding order is canceled.

B. PHASOR ESTIMATION

The objective of the error phasor estimation is to identify the error phasors based on the measured torque. This can be interpreted as a transition from the time to the frequency domain. It can be achieved by recursively solving a linear regression problem in a least-squares sense with the help of an RLS algorithm which is described in the following.

The torque (1) can be reformulated as a linear regression problem

$$\psi[k] = \boldsymbol{\xi}[k]^{\text{T}} \boldsymbol{\theta} \tag{6}$$

with the measured variable $\psi[k] = T_{\text{meas}}[k]$, the regressor vector, that contains the known reference oscillation signals

$$\boldsymbol{\xi}[k] = \begin{bmatrix} \cos(p_1 \varepsilon[k]) \\ \sin(p_1 \varepsilon[k]) \\ \cos(p_2 \varepsilon[k]) \\ \sin(p_2 \varepsilon[k]) \\ \vdots \\ \cos(p_r \varepsilon[k]) \\ \sin(p_r \varepsilon[k]) \\ 1 \end{bmatrix}, \tag{7}$$

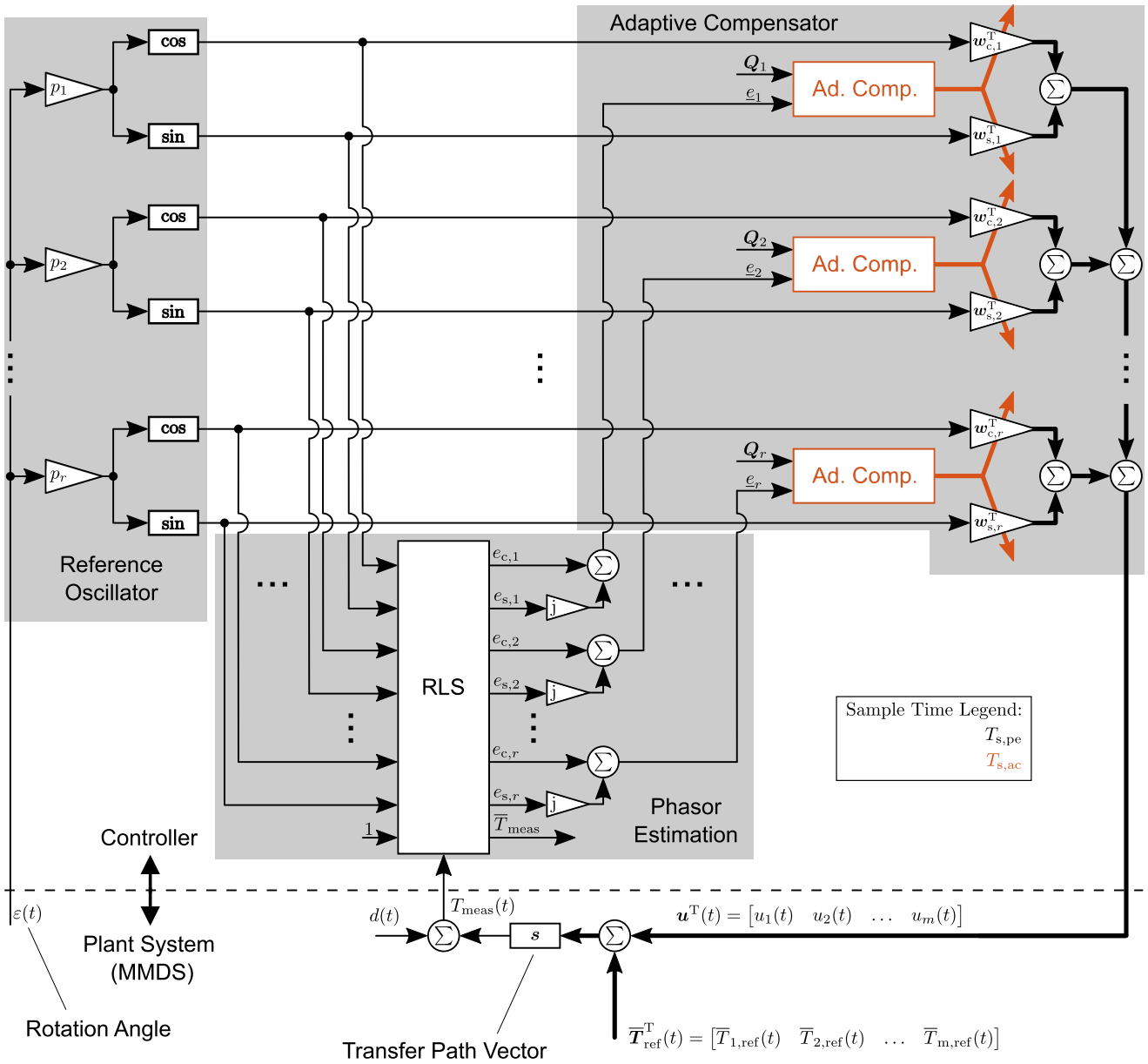

FIG. 4. **Overall compensation scheme.**

with ε as measured rotor angle of one of the MMDS's motors and the unknown parameter vector

$$\boldsymbol{\theta}^{\mathrm{T}} = \begin{bmatrix} e_{\mathrm{c},1} & e_{\mathrm{s},1} & e_{\mathrm{c},2} & e_{\mathrm{s},2} & \dots & e_{\mathrm{c},r} & e_{\mathrm{s},r} & \overline{T}_{\mathrm{meas}} \end{bmatrix}. \tag{8}$$

By utilizing the RLS method as an adaptive filter for the phasor estimation, the parameter vector, which is defined by the phasors (cf. (8)), is recursively corrected with each new torque measurement. The calculations that must be executed in each iteration can be formulated as following [43]

$$\boldsymbol{\gamma}[k] = \frac{\boldsymbol{P}[k]\boldsymbol{\xi}[k+1]}{\lambda_{\mathrm{pe}} + \boldsymbol{\xi}^T[k+1]\boldsymbol{P}[k]\boldsymbol{\xi}[k+1]}, \tag{9a}$$

$$\hat{\boldsymbol{\theta}}[k+1] = \hat{\boldsymbol{\theta}}[k] + \boldsymbol{\gamma}[k]\left(\psi[k+1] - \boldsymbol{\xi}[k+1]^T\hat{\boldsymbol{\theta}}[k]\right), \tag{9b}$$

$$\boldsymbol{P}[k+1] = \frac{1}{\lambda_{\mathrm{pe}}}\left(\boldsymbol{I} - \boldsymbol{\gamma}[k]\boldsymbol{\xi}^T[k+1]\right)\boldsymbol{P}[k]. \tag{9c}$$

Above, $\boldsymbol{P}$ is a matrix proportional to the covariance matrix $\mathrm{Cov}(\hat{\boldsymbol{\theta}}, \hat{\boldsymbol{\theta}})$ of the estimated parameter vector and the forgetting factor $0 < \lambda_{\mathrm{pe}} < 1$ is a weighting factor that assigns a lower weighting to past measurements for smaller values of λ_{pe}. In (9a) a correction term is calculated that is used to update the parameter vector $\hat{\boldsymbol{\theta}}$ and the matrix $\boldsymbol{P}$. An initial parameter vector $\hat{\boldsymbol{\theta}}[0]$ and an initial matrix $\boldsymbol{P}[0]$ must be specified in addition. To prevent multicollinearities of the regressors and, therefore, a rank deficient matrix $\boldsymbol{P}$, a persistent excitation of the RLS must be ensured. For the chosen regressors (7)

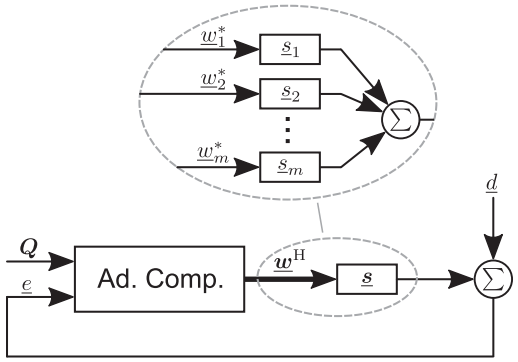

FIG. 5. Block diagram of the plant system from the perspective of the adaptive compensator for one frequency order.

a persistent excitation is guaranteed and, therefore, multicollinearities are prevented because the regressors are linearly independent for different order numbers p_i and a time-varying rotor angle ε. However, at standstill and for low speed the time variation of the rotor angle is not sufficient to ensure persistent excitation. For this reason the compensation scheme is deactivated when the speed of the MMDS falls under a certain speed threshold n_{pe}. This speed threshold may be chosen heuristically. Instead, it can also be calculated a priori for given order numbers p_i and a given forgetting factor λ_{pe}, since the condition number of $\boldsymbol{P}$ in (9c), which is a measure of the collinearity of the regressors $\boldsymbol{\xi}$, depends only on the forgetting factor and on the regressors and not on measurements of the actual MMDS.

C. ADAPTIVE COMPENSATOR

To cancel r harmonic torque orders, r adaptive compensators are utilized which are independent of each other. For concise presentation, the adaptive compensator is considered on the basis of a single order. The extension to several orders can be realized analogously. The adaptive compensator approach can be split into an identification task and into the determination of optimal weights which is described in the following two subsections. The basis for the identification of the transfer path and the disturbance is represented by (5). Here, a steady-state oscillation also called harmonic steady state is assumed, i.e., the MMDS is not transiently excited by changing mean reference torques or changing disturbances and compensation reference torques in amplitude, phase, or frequency. The block diagram of the adaptive compensator including the plant model (5) for one order is shown in Fig. 5.

TRANSFER PATH AND DISTURBANCE IDENTIFICATION

Since (5) is the basis for the adaptive compensator, the sampling rate $T_{\mathrm{s,ac}}$ of the adaptive compensator must be sufficiently low such that the system returns to a quasi-steady state within one sampling interval after a change of the weight vector which will transiently excite the MMDS. Assuming that the unknown transfer paths $\underline{\boldsymbol{s}}$ and the disturbances $\underline{d}$ do not change, (5) can be represented as

$$\underline{e}[n] = \underline{\boldsymbol{w}}^{\mathrm{H}}[n]\underline{\boldsymbol{s}} + \underline{d} \tag{10}$$

on the slower task of the adaptive compensator with sampling index n. In a first step, the transfer path is identified. To eliminate the disturbance $\underline{d}$ for the identification of the transfer path, the difference of (10) between the time steps n and $n-1$ is calculated

$$\begin{aligned}\Delta\underline{e}[n] &= \Delta\underline{\boldsymbol{w}}^{\mathrm{H}}[n]\underline{\boldsymbol{s}} \\ &= \sum_{i=1}^{r} \Delta\underline{w}_i^*[n]\underline{s}_i\end{aligned} \tag{11}$$

with the error difference $\Delta\underline{e}[n] := \underline{e}[n] - \underline{e}[n-1]$ and the weight difference $\Delta\underline{\boldsymbol{w}}^{\mathrm{H}}[n] := \underline{\boldsymbol{w}}^{\mathrm{H}}[n] - \underline{\boldsymbol{w}}^{\mathrm{H}}[n-1]$. The adaptive compensator changes only the i-th element of the weight vector with $i = \mathrm{mod}(n, m)$ per time step n such that (11) can be further simplified to

$$\Delta\underline{e}[n] \overset{\Delta\underline{w}_j^*[n]=0,\ j\neq i}{=} \Delta\underline{w}_i^*[n]\underline{s}_i \tag{12}$$

decoupling the identification of the elements of the transfer path vector $\underline{\boldsymbol{s}}$. Here, (12) can be interpreted as a linear regression problem with a complex known measurement $\Delta\underline{e}[n]$ and regressor $\Delta\underline{w}_i^*[n]$. For every i unknown transfer path $\underline{s}_i$, a single-weight complex-valued RLS (cRLS) is used for solving the regression problem and, therefore, to identify $\underline{s}_i$. The calculations that must be executed in each iteration can be formulated as follows [35]

$$\underline{\gamma}_i[n] = \frac{\Delta\underline{w}_i^*[n]}{\lambda_{\mathrm{ac}}\sigma_i^2[n-1] + |\Delta\underline{w}_i^*[n]|^2}, \tag{13a}$$

$$\hat{\underline{s}}_i[n] = \hat{\underline{s}}_i[n-1] + \underline{\gamma}_i^*[n]\left(\Delta\underline{e}[n] - \Delta\underline{w}_i^*[n]\hat{\underline{s}}_i[n-1]\right), \tag{13b}$$

$$\sigma_i^2[n] = \lambda_{\mathrm{ac}}\sigma_i^2[n-1] + |\Delta\underline{w}_i^*[n]|^2. \tag{13c}$$

Above, σ_i is the estimated variance of the estimated transfer path $\hat{\underline{s}}_i$. The estimated variance of the transfer path and the estimated transfer path itself are updated with a correction term (13a) whereby the forgetting factor $0 < \lambda_{\mathrm{ac}} < 1$ gives more or less weight to previous measurements for the identification process similar to the case of the RLS for the phasor estimation, cf. Section II-B. Furthermore initial values $\sigma_i[0]$ and $\hat{\underline{s}}_i[0]$ must be specified. It is worth noting that for the single-weight cRLS (13) only scalar quantities appear in (13a)-(13c) which leads to a minor computational effort to estimate $\hat{\underline{s}}_i$.

By continually identifying the transfer path vector, the disturbance $\underline{d}$ can be estimated using (10) and the transfer path estimate $\hat{\underline{\boldsymbol{s}}}$

$$\hat{\underline{d}}[n] = \underline{e}[n] - \underline{\boldsymbol{w}}^{\mathrm{H}}[n]\hat{\underline{\boldsymbol{s}}}[n]. \tag{14}$$

OPTIMAL WEIGHT DETERMINATION

The objective of the weight selection is to eliminate the error $\underline{e}[n+1]$ via a suitable selection of the weight vector for the

next sampling instant $n+1$ based on the estimates of the transfer path and disturbance

$$\underline{e}[n+1] = 0 = \underline{\boldsymbol{w}}^{\mathrm{H}}[n+1]\underline{\hat{\boldsymbol{s}}}[n] + \underline{\hat{d}}[n]. \tag{15}$$

However, using (15), the weight vector cannot be uniquely determined in general because it is an overdetermined equation with m unknown complex weight vector elements. For this reason it is advantageous to minimize a weighted Euclidean norm of the weight vector under the constraint that the error is eliminated. This objective leads to minimal possible weighted control effort resulting in following quadratic program with a linear equality constraint:

$$\min_{\underline{\boldsymbol{w}}[n+1]} \underline{\boldsymbol{w}}^{\mathrm{H}}[n+1]\boldsymbol{Q}[n]\underline{\boldsymbol{w}}[n+1] \tag{16a}$$

$$\text{s.t.} \quad 0 = \underline{\boldsymbol{w}}^{\mathrm{H}}[n+1]\underline{\hat{\boldsymbol{s}}}[n] + \underline{\hat{d}}[n]. \tag{16b}$$

Here, $\boldsymbol{Q} \in \mathbb{R}^{m\times m}$ is a positive-definite matrix that acts as tuning parameter of the compensator

$$\boldsymbol{Q}[n] = \begin{bmatrix} q_1[n] & 0 & \cdots & 0 \\ 0 & q_2[n] & \ddots & \vdots \\ \vdots & \ddots & \ddots & 0 \\ 0 & \cdots & 0 & q_m[n] \end{bmatrix}. \tag{17}$$

It is advantageous to choose $\boldsymbol{Q}$ as a diagonal matrix because its components q_i can be used to adjust the participation of the i-th drive for the compensation of the chosen order. By increasing the value q_i the i-th drive will participate less on the compensation task and the other drives have to take over more of it and vice versa. For example, those drives providing a rather high average torque should only contribute marginally to the harmonic compensation to reduce power losses which increase (approximately) quadratically with the torque demand per drive.

Due to the structure of (16), an analytical and, therefore, a computationally efficient solution exists compared to the solution that is found by iterative numerical optimization problem solvers. This analytic solution can be found with the help of a Lagrangian function:

$$\underline{\boldsymbol{w}}_{\mathrm{opt}}[n+1] = -\frac{\underline{\hat{d}}[n]\boldsymbol{Q}^{-1}[n]\underline{\hat{\boldsymbol{s}}}^{*}[n]}{\underline{\hat{\boldsymbol{s}}}^{\mathrm{H}}[n]\boldsymbol{Q}^{-1}[n]\underline{\hat{\boldsymbol{s}}}[n]}. \tag{18}$$

Instead of using the entire optimal weight vector $\underline{\boldsymbol{w}}_{\mathrm{opt}}[n+1]$, only one element of the weight vector $\underline{\boldsymbol{w}}[n]$ is replaced by an element $\underline{w}_{\mathrm{opt},i+1}[n+1]$ of the optimized weight vector otherwise (12) is not fulfilled and the transfer paths can no longer be identified decoupled from each other. Hence, the weight vector at time step $n+1$ results to

$$\underline{\boldsymbol{w}}[n+1] = \begin{bmatrix} \underline{w}_1[n] \\ \vdots \\ \underline{w}_i[n] \\ \underline{w}_{\mathrm{opt},i+1}[n+1] \\ \underline{w}_{i+2}[n] \\ \vdots \\ \underline{w}_m[n] \end{bmatrix}. \tag{19}$$

The real-valued weights $\boldsymbol{w}_{\mathrm{c}}$, $\boldsymbol{w}_{\mathrm{s}}$ that are multiplied with the reference oscillation signals, cf. (3), are than given by:

$$\boldsymbol{w}_{\mathrm{c}}[n+1] = \mathrm{Re}\left(\underline{\boldsymbol{w}}^{*}[n+1]\right), \ \boldsymbol{w}_{\mathrm{s}}[n+1] = \mathrm{Im}\left(\underline{\boldsymbol{w}}^{*}[n+1]\right). \tag{20}$$

The calculation steps of the adaptive compensator including the identification and weight selection task are summarized with the help of a structogram in Fig. 6. For one adaptive compensator to damp one harmonic order m single-weight cRLS (13) must be calculated and one QP (16) needs to be solved with (18) analytically. This results in rm single-weight cRLS (13) and r QPs (16) that need to be solved to damp r torque harmonics with m motors.

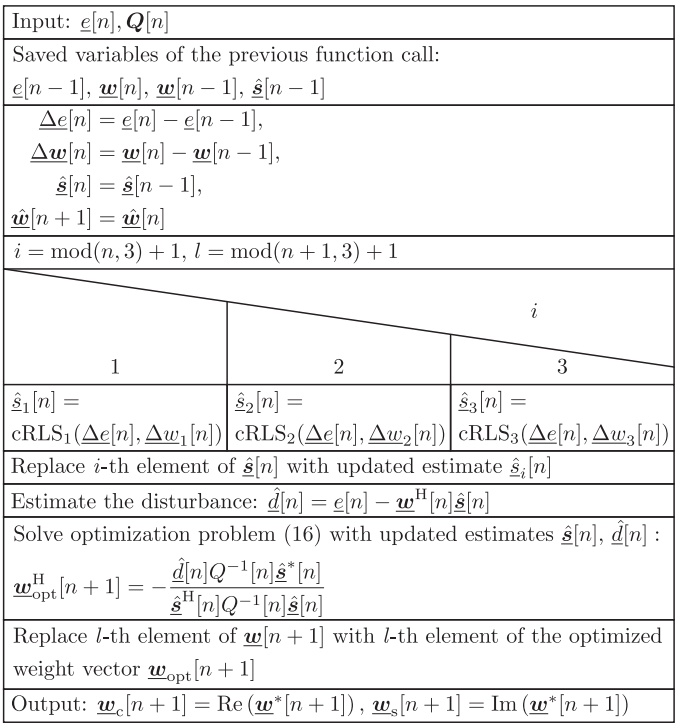

FIG. 6. Structogram of one adaptive compensator for $m = 3$ motors of the MMDS.

D. TUNING PARAMETERS

The proposed approach includes the following tuning parameters regarding the phasor estimation and reference oscillator:

1) Sampling time $T_{s,pe}$ of the reference oscillator and RLS phasor estimation
2) Forgetting factor λ_{pe} of the RLS phasor estimator.

Due to the Whittaker-Kotelnikow-Shannon (WKS) sampling theorem, the sampling time $T_{s,pe}$ must be chosen such that resulting sampling frequency is greater than twice the highest frequency that should be compensated. If significant oscillations exist that are not intended for compensation with frequencies that violate the WKS sampling theorem, two options are available to fulfill the WKS sampling theorem. Either the signal portion with frequencies above $0.5/T_{s,pe}$ must be filtered out by an analog low-pass filter, or $T_{s,pe}$ must be reduced further.

The forgetting factor λ_{pe} is used to adjust the dynamics of the phasor estimation. Here, a trade-off between noise suppression by a high forgetting factor and fast parameter tracking by a small forgetting factor must be chosen. However, the forgetting factor must be selected sufficiently small such that the RLS parameter tracking is fast enough to return to a steady-state estimation within one sampling interval $T_{s,ad}$ after a change of the compensation signal by the adaptive compensators.

For the adaptive compensators the following tuning parameters are available:

1) Sampling time $T_{s,ac}$,
2) Forgetting factor λ_{ac},
3) Weighting matrices $\boldsymbol{Q}_{\{1,2,\ldots,r\}}$.

Since the underlying adaptive compensators assume a steady state of oscillation, the sampling time $T_{s,ad}$ must be chosen sufficiently large to ensure that a change in the compensation signal causes the system to return to a steady state of oscillation within one sampling interval $T_{s,ad}$. However, in order to be able to react quickly to operating point changes, the sampling interval $T_{s,ad}$ should be chosen short. Here, a sampling interval of roughly 3 to 5 times the slowest time constant of the system seems appropriate. Although the weight vector $\underline{\boldsymbol{w}}_{opt}$ that defines the compensation signals is kept constant for $T_{s,ad}$, the mean reference torques $\overline{\boldsymbol{T}}_{ref}$ of the MMDS motor drives are allowed to change with the sampling time of the inverters. For this reason, the torque control dynamic to fulfill the main drive task is not reduced by the compensation algorithm.

The forgetting factor λ_{ad} is used to adjust the dynamics of the transfer path estimations. Here, also a trade-off between noise suppression by a high forgetting factor and fast transfer path tracking by a small forgetting factor must be chosen.

If the transfer paths from the individual MMDS's drives to the torque sensor are of similar magnitude, $\boldsymbol{Q} = I$ is a choice with that the individual drives participate on the compensation task with similar magnitude. If the distribution of the compensation task should be changed, this can be done by increasing or decreasing the diagonal elements of $\boldsymbol{Q}$ at runtime. Furthermore, different weight matrices $\boldsymbol{Q}_{\{1,2,\ldots,r\}}$ can be chosen for each order that is to be compensated.

TABLE I Individual Motors of the MMDS

#	Motor	Rated torque in Nm	Rated power in kW
1	Siemens 1PH8103	34	6.3
2	Siemens 1PH8103	34	6.3
3	Siemens 1PH8105	44	8.0
4	Siemens 1PH8101	23	4.3

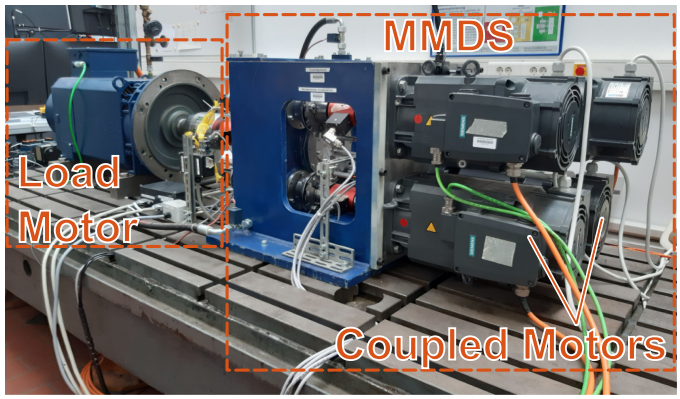

FIG. 7. MMDS test bench with the two coupled motors (the other two are mechanically decoupled) for the experimental investigations.

The advantage of the proposed compensation approach is that no complex offline system identification of transfer functions and disturbances is required, since these are identified online. For this reason, no model-based controller synthesis is intended which means that the tuning parameters have to be determined empirically on the test bench. However, each tuning parameter and its impact on the control approach can be interpreted intuitively such that initial value guesses are straightforward. A superimposed automatic tuning procedure using numerical optimization or rule-based heuristics can be added as well.

III. EXPERIMENTAL INVESTIGATION

A. EXPERIMENTAL TEST SETUP

To prove the torque compensation capability of the proposed approach, an MMDS test bench consisting of four torque-controlled induction motor drives (Table I), coupled via a cumulative gear in combination with a torque sensor (KTR Dataflex 42/1000 [44]) on the output shaft, is utilized. Furthermore, a speed-controlled induction motor drive (Siemens 1PA6186), which acts as load, is mechanically coupled to the gear's output shaft. Fig. 7 depicts the test bench configuration. The MMDS's electric cabinet consists of Siemens SINAMICS S120 inverter modules with integrated torque controllers. These inverter modules are operated at a switching frequency of 4 kHz. Furthermore a dSPACE DS1006 real-time hardware and a related PC are connected via a ProfiBus-DP link. For ease of flexibility during software development with MATLAB/Simulink, the proposed compensator approach is implemented on the dSPACE system, which sends the reference compensation torques to the Siemens inverter modules.

TABLE II Tuning Parameters of the Compensation Scheme

Phasor estimation		
Sampling time	$T_{\mathrm{s,pe}}$	0.4 ms
Forgetting factor	λ_{pe}	0.98
Speed Threshold	n_{pe}	20 1/min
Adaptive compensator		
Sampling time	$T_{\mathrm{s,ac}}$	0.5 s
Forgetting factor	λ_{ac}	0.9
Weighting matrix (if not specified)	$\boldsymbol{Q}_{\{1,2,\ldots,r\}}$	$\boldsymbol{I}$

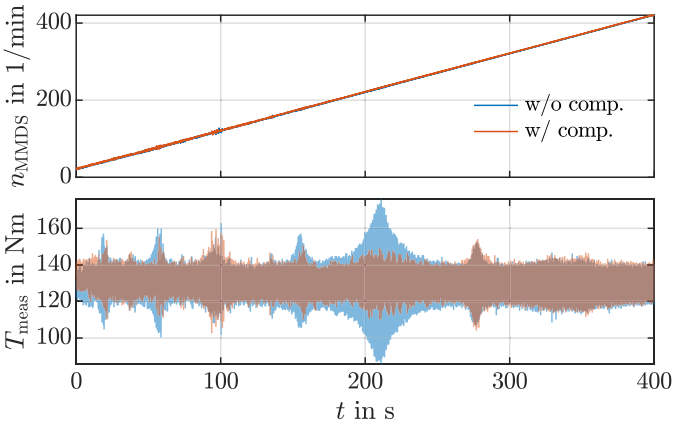

FIG. 8. Speed ramp to the nominal speed and corresponding torque trajectories of the MMDS's shaft with and without activated compensation scheme.

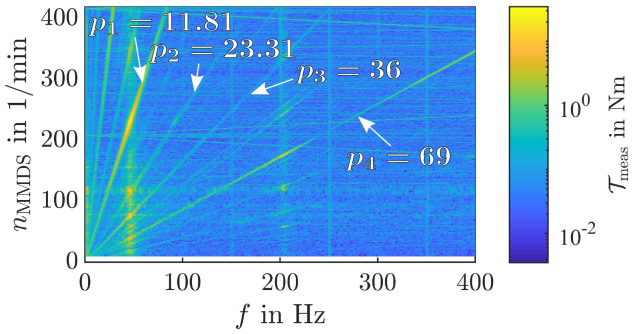

FIG. 9. Campbell diagram of the torque and speed trajectories of Fig. 8 without activated compensation scheme and marked dominant orders (intended to be compensated).

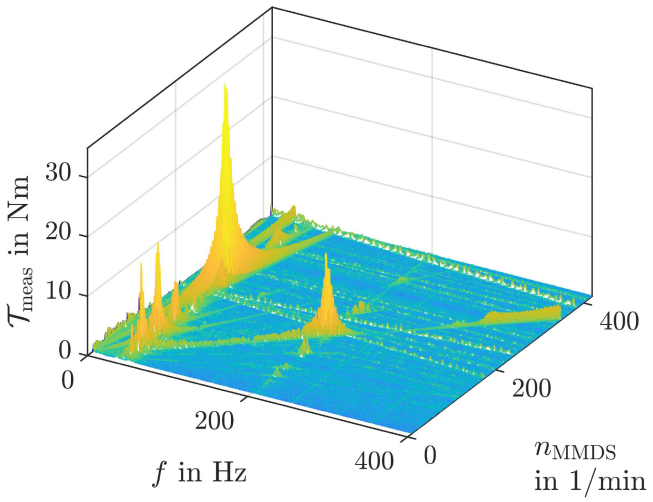

FIG. 10. 3D waterfall Campbell diagram of the torque and speed trajectories of Fig. 8 with deactivated compensation scheme.

The utilized MMDS test bench offers the possibility to mechanically decouple individual motors from the cumulative gear such that motors that are not needed (e.g., due to temporary lower torque requirement) can be decoupled in order to increase the overall efficiency. For all subsequent experimental investigations this possibility was used with motors 1 and 2 coupled and motors 3 and 4 permanently decoupled. The tuning parameters of the compensation scheme for the following experiments are listed in Table II. The execution time for the implemented compensation algorithm on the utilized dSPACE DS1006-03 processor board with an AMD Opteron single-core processor running at 2.6 GHz was 3.7 µs. Here, up to four orders were compensated. Due to this low computational demand, the proposed approach is ideally suited for the implementation on low-cost microcontrollers as well.

B. SPEED RAMP INVESTIGATION

In order to gain insight into the torque oscillation phenomena of the MMDS, a speed ramp from nearly zero to nominal speed was forced by the load machine. This allows the stationary compensation capability of the proposed approach to be investigated, since the speed only changes slowly and thus quasi-stationary states can be assumed. For this scenario the two torque-controlled drives 1 and 2 of the MMDS applied 17 Nm each. In Fig. 8 the corresponding speed n_{MMDS} and measured torque trajectories of the MMDS's output shaft with deactivated compensation scheme are depicted. Here, significant torque oscillations can be seen. To investigate the frequency content of the torque signal of Fig. 8 as a function of the speed, a Campbell diagram of the torque and speed signals without activated compensation scheme of Fig. 8 is shown, see Fig. 9. Here, $\mathcal{T}_{\mathrm{meas}}(f)$ denotes the amplitude of $T_{\mathrm{meas}}(t)$ for the corresponding frequency f at speed n_{MMDS}. With the help of the Campbell diagram, two significant resonance frequencies of the MMDS can be identified at approx. 50 Hz and approx. 200 Hz. If the lines of constant orders (lines through the origin of the Campbell diagram) of the disturbance intersect these resonance frequencies, the MMDS is excited and torque oscillations amplify. In the Campbell diagram shown in Fig. 9 resonance frequencies as well as orders can be easily identified. For a better depiction of the peak heights, a 3D waterfall diagram can be viewed in Fig. 10 which is based on the same measurement as 9. Here, significant peaks can be detected when the four orders $p_i = \{11.81,\ 23.32,\ 36,\ 69\}$ intersect the resonance frequency at approx. 50 Hz and when the order $p_4 = 69$ intersects the second resonance frequency at approx. 200 Hz.

By compensating the orders $p_i = \{11.81,\ 23.32,\ 36,\ 69\}$ a significant reduction of the torque oscillations can be

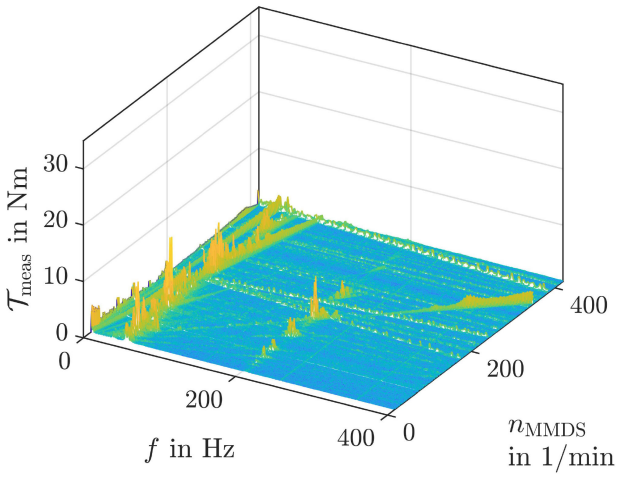

FIG. 11. 3D waterfall Campbell diagram of the torque and speed trajectories of Fig. 8 with activated compensation scheme.

achieved, see Figs. 9 and 11, especially when $p_1 = 11.81$ intersects the first resonance frequency at approx. 50 Hz and when $p_4 = 69$ intersects the second resonance frequency at approx. 200 Hz. Torque oscillations that arise at frequencies greater than 250 Hz remain uncompensated because the adaptive compensators were deactivated for such excitation signals. This is caused by the rapidly increasing amplitudes of the compensation signals with increasing frequency due to the low-pass filter effect of the torque controller and the mechanical inertia. Because of a software limitation of the reference torque in the used Siemens industrial inverters, these high amplitudes would lead to a situation where the mean reference torque can no longer be provided. For this reason, it is preferable to use a maximum frequency to be canceled as threshold for the adaptive compensators. This threshold frequency is of course dependent on the respective mechanical system as well as the actuators and their torque controllers.

C. INVESTIGATION OF WEIGHTING MATRIX VARIATION

Due to the formulation of the optimization problem (16), one weight matrix $\boldsymbol{Q}_i$ per order p_i is available as tuning parameter of the proposed approach. With these matrices $\boldsymbol{Q}_i$ the participation of the respective drives of the MMDS on the compensation task of the order p_i can be changed at runtime which gives additional flexibility. The influence of a change in the weight matrix $\boldsymbol{Q}_i$ on the measured torque T_{meas}, the instantaneous electrical power of the induction machines $p_{\{1,2\}}$ measured by the inverter modules, and the reference compensation torques $u_{\{1,2\}}$ is investigated in the following. For this purpose, the operating point from the previous chapter was used, at which the highest oscillation amplitude was generated (cf. Fig. 10). For this investigation the speed was kept constant by the load machine at $n_{\text{MMDS}} = 230\,\text{min}^{-1}$. Here, only the order $p = 11.81$ leads to significant excitation of torque harmonics by intersecting the first resonance frequency at approx. 50 Hz. For this reason, only the order $p = 11.81$ was compensated

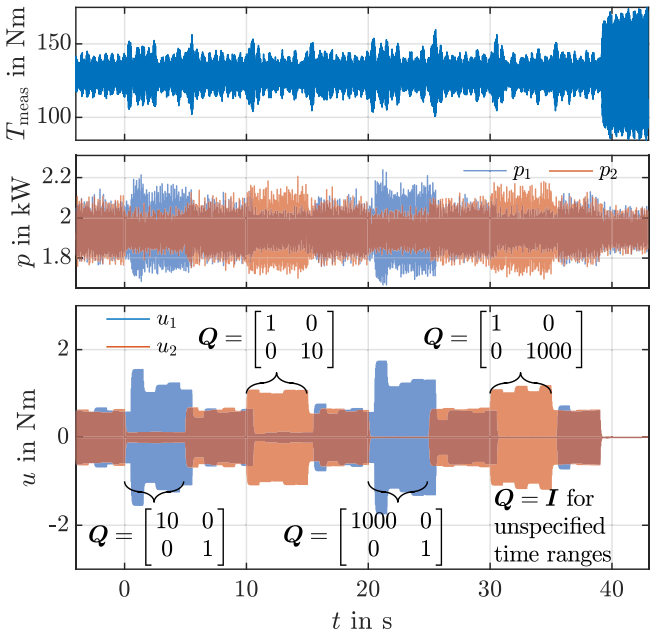

(a) Influence of the weighting matrix $\boldsymbol{Q}$ on the measured torque T_{meas} and the reference compensation torques $u_{\{1,2\}}$ for $\overline{T}_{1,\text{ref}} = \overline{T}_{2,\text{ref}} = 17\,\text{Nm}$ and $n_{\text{MMDS}} = 230\,\text{min}^{-1}$

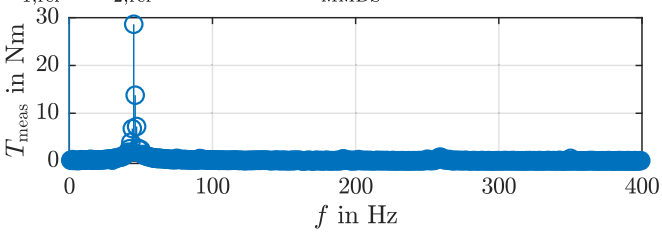

(b) Fourier analysis for the time range $t \in [40, 41]$ s of Fig. 12a with deactivated compensation scheme resulting in a total harmonic torque distortion of $\text{THD}_\text{T} = 0.268$

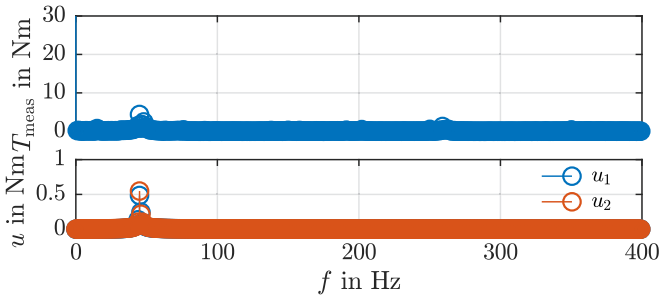

(c) Fourier analysis for the time range $t \in [-1, 0]$ s of Fig. 12a with activated compensation scheme resulting in a total harmonic torque distortion of $\text{THD}_\text{T} = 0.054$

FIG. 12. Change of the weighting matrix $\boldsymbol{Q}$ at a constant speed of $n_{\text{MMDS}} = 230\,\text{min}^{-1}$ and Fourier analysis with deactivated and activated compensation scheme.

in this scenario. To investigate the weighting matrix's influence, the elements of the main diagonal of $\boldsymbol{Q}$ are changed every $t = 5$ s, see Fig. 12(a). At $t = 39$ s the compensation scheme is deactivated which leads to a significant increase of the torque oscillation amplitude. The compensation capability

of the proposed method can be also proven in the frequency domain with the help a of Fourier analysis with deactivated compensation scheme (cf. Fig. 12(b)) and activated scheme (cf. Fig. 12(c)). On the basis of the Fourier analysis the total harmonic distortion (THD), which is a suitable measure to assess the compensator's oscillation-rejection capability, can be calculated via

$$\mathrm{THD_T} = \frac{\sqrt{\sum_{h\neq 0} \mathcal{T}_{h,\mathrm{meas}}^2}}{\sqrt{2}\mathcal{T}_{0,\mathrm{meas}}}. \tag{21}$$

Here, the amplitudes $\mathcal{T}_{h,\mathrm{meas}}$ are the harmonic components and $\mathcal{T}_{0,\mathrm{meas}}$ the mean of the measured torque T_{meas}. The factor $\sqrt{2}$ results, since $\mathcal{T}_{h,\mathrm{meas}}$ are amplitudes and not effective values. By deactivating the compensation scheme the THD increased from $\mathrm{THD_T} = 0.054$ to $\mathrm{THD_T} = 0.268$ which corresponds to a relative reduction of the THD of 80 % with the proposed compensation scheme in this operating point.

For $\boldsymbol{Q} = \boldsymbol{I}$ the amplitudes of the reference compensation torques are in the same order of magnitude, see Fig. 12(a). This is an indication that the transfer paths $\underline{s}_1$ and $\underline{s}_2$ are also in the same order of magnitude. As both drives including their torque controllers are identical and a symmetrical mechanical construction of the MMDS is given this seems to be plausible. By increasing q_i on the diagonal of $\boldsymbol{Q}$, the i-th drive contributes less to the compensation task while the other drive takes over such that the overall compensation capability can be maintained. The value q_i can be increased to such extent, that from a practical point of view the i-th drive does not participate in the compensation task at all (cf. Fig. 12(a)) which can be advantageous if the i-th drive is operated at its torque or voltage limit. The more a drive participates on the compensation task, the more its instantaneous electrical power consumption fluctuates, see Fig. 12(a). However, the mean momentary electrical power remains constant since mainly reactive power is required for vibration compensation of the weakly damped mechanical system. No significant increase in power loss due to activated compensation was detected. After a change of the weight matrix $\boldsymbol{Q}$ an increased torque oscillation can be observed for one sampling instant n. This is because only one of the two entries of $\underline{\boldsymbol{w}}[n+1]$ is based on the changed weighting matrix $\boldsymbol{Q}[n]$. The other element of $\underline{\boldsymbol{w}}[n+1]$ is based on the old $\boldsymbol{Q}[n-1]$ because only one element of the weight vector $\underline{\boldsymbol{w}}[n+1]$ is updated per sampling step. This way the decoupled identification of the transfer paths can be maintained. By changing $\boldsymbol{Q}$, the constraint (16b) cannot be fulfilled in general for the actual applied weight $\underline{\boldsymbol{w}}[n+1]$ for the following $m-1$ sampling instants.

D. EVALUATION DURING TRANSIENTS

In Section III-B the stationary compensation capability of the proposed approach was shown for constant reference torques $\overline{T}_{x,\mathrm{ref}}$ and a quasi-stationary speed. In order to investigate the compensation capability also for changing reference torque $\overline{T}_{x,\mathrm{ref}}(t)$ and speed $n_{\mathrm{MMDS}}(t)$, a sinusoidal reference torque of 2 Hz for both drives was superimposed to the operating point

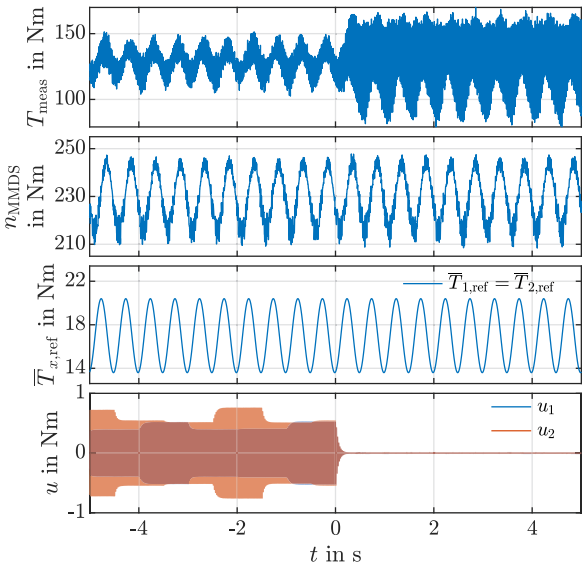

(a) Measured torque T_{meas} for sinusoidal reference torques $\overline{T}_{1,\mathrm{ref}}(t) = \overline{T}_{2,\mathrm{ref}}(t)$ with activated ($t \leq 0\,\mathrm{s}$) and deactivated ($0\,\mathrm{s} < t$) compensation scheme

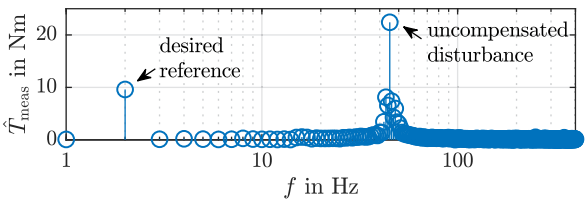

(b) Fourier analysis for the time range $t \in [2, 3]$ s of Fig. 13a with deactivated compensation scheme

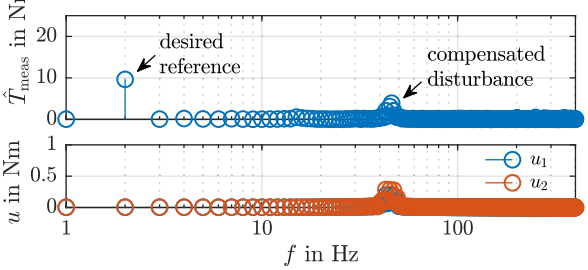

(c) Fourier analysis for the time range $t \in [-3, -2]$ s of Fig. 13a with activated compensation scheme

FIG. 13. Analysis of activated and deactivated compensation scheme during sinusoidal speed changes due to additive sinusoidal reference torques of the MMDS's drives.

conditions of Section III-C with $\boldsymbol{Q} = \boldsymbol{I}$, see. Fig. 13(a). The harmonic content with the deactivated compensation scheme of the measured output torque of the MMDS can be seen in Fig. 13(b). Here, the desired harmonic at 2 Hz due to the sinusoidal reference torques and the undesired torque oscillations at approx. 50 Hz are present. By activating the compensation scheme the undesired torque oscillations are damped by the compensation signals $u_{1,2}$ and the desired harmonic at 2 Hz remains unaffected. For more transient scenarios e.g., step-like changes of the load torque and the reference torque of the MMDS, the proposed approach offers no advantages, which

is due to its steady-state assumption. Hence, the compensation scheme can be deactivated during highly transient operation.

IV. CONCLUSION AND OUTLOOK

It has been shown that an adaptive compensation of measured torque oscillations of the MMDS is feasible for quasi-steady-state oscillations by adding harmonic components to the reference torques of the MMDS's drives. For the computation of the harmonic reference torques no time-consuming offline system identification of the MMDS is required thanks to the online transfer path identification. This leads to an adaptation of the compensator to quasi-stationary operating points whereby experimentally a relative reduction of the torque's THD of up to 80% could be achieved. Furthermore, the contribution of the respective drives of the MMDS to the compensation task can be configured at runtime using a weighting matrix, which provides additional flexibility.

In the future, it needs to be investigated whether the expensive measurement using a torque sensor at the shaft of the MMDS can be avoided. Here, cost-efficient microphones or accelerometers placed at suitable locations in or outside the MMDS could be promising candidates. Moreover, automatic tuning procedures reducing the application effort are subject to future research work.

REFERENCES

[1] L. Sedlmeier and H. Skride, *Kostenwirkung Der Modularisierung (KosMo)*, Ser. FVA-Heft. Forschungsvereinigung Antriebstechnik E.v. (FVA), 2013, no. 1081.

[2] Verband DeutscherMaschinen-undAnlagenbau e.V., (VDMA) and McKinsey & Company, *Erfolgsmuster Und Trends in Der Deutschen Antriebstechnik - Handlungsansätze Für Mehr Wachstum Und Profitabilität*, 2014.

[3] M. Strop and D. Zimmer, "Intelligent operating strategy for an internal rubber mixer's multi-motor drive system based on artificial neural network," in *Proc. IEEE 21st Int. Conf. Emerg. Technol. Factory Automat.*, 2016, pp. 1–9.

[4] J. Wei, Q. Sun, W. Sun, X. Ding, W. Tu, and Q. Wang, "Load-sharing characteristic of multiple pinions driving in tunneling boring machine," *Chin. J. Mech. Eng.*, vol. 26, no. 3, pp. 532–540, 2013.

[5] H. Zhang, M. Wang, Q. Han, and W. Sun, "Dynamic behaviors of the cutterhead driving system in tunneling boring machine with impact," *Proc. Inst. Mech. Engineers*, *Part C: J. Mech. Eng. Sci.*, vol. 230, pp. 2427–2437, 2016.

[6] C. A. Michael and A. N. Safacas, "Dynamic and vibration analysis of a multimotor DC drive system with elastic shafts driving a tissue paper machine," *IEEE Trans. Ind. Electron.*, vol. 54, no. 4, pp. 2033–2046, Aug. 2007.

[7] P. V. Krot, "Dynamical processes in a multi-motor gear drive of heavy slabbing mill," *J. Vibroeng.*, vol. 21, pp. 2064–2081, 2019.

[8] B. Jeftenic, M. Bebic, and S. Statkic, "Controlled multi-motor drives," in *Proc. Int. Symp. Power Elect., Elect. Drives, Automat. Motion, SPEEDAM*, 2006, pp. 1392–1398.

[9] M. Bächler, N. Khoury, and J. Weston, "Drive systems for vertical roller mills," in *Proc. IEEE-IAS/PCA Cement Ind. Tech. Conf.*, 2017, pp. 1–11.

[10] T. Vogt, A. Peters, N. Fröhleke, J. Böcker, and S. Kempen, "Power profile based selection and operation optimization of parallel-connected power converter combinations," in *Proc. Int. Power Electron. Conf. (IPEC-Hiroshima 2014 - ECCE ASIA)*, 2014, pp. 2887–2892.

[11] F. dell'Isola, C. Maurini, and M. Porfiri, "Passive damping of beam vibrations through distributed electric networks and piezoelectric transducers: Prototype design and experimental validation," *Smart Mater. Struct.*, vol. 13, no. 2, 2004, Art. no. 299.

[12] C. D. Johnson, "Design of passive damping systems," *J. Vib. Acoust.*, vol. 117, no. B, pp. 171–176, 1995.

[13] D. D. L. Chung, "Review: Materials for vibration damping," *J. Mater. Sci.*, vol. 36, pp. 5733–5737, 2001.

[14] M. J. Crosby and D. C. Karnopp, "The active damper: A new concept for shock and vibration control," *Shock Vib. Bull.*, vol. 43, no. 4, pp. 119–133, 1973.

[15] F.-Y. Huang, T. Semba, W. Imaino, and F. Lee, "Active damping in HDD actuator," *IEEE Trans. Magn.*, vol. 37, no. 2, pp. 847–849, Mar. 2001.

[16] M. Morandin, S. Bolognani, and A. Faggion, "Active torque damping for an ice-based domestic CHP system with an SPM machine drive," *IEEE Trans. Ind. Appl.*, vol. 51, no. 4, pp. 3137–3146, Jul./Aug. 2015.

[17] S. N. Vukosavic and M. R. Stojic, "Suppression of torsional oscillations in a high-performance speed servo drive," *IEEE Trans. Ind. Electron.*, vol. 45, no. 1, pp. 108–117, Feb. 1998.

[18] N. Amann, J. Böcker, and F. Prenner, "Active damping of drive train oscillations for an electrically driven vehicle," *IEEE/ASME Trans. Mechatronics*, vol. 9, no. 4, pp. 697–700, Dec. 2004.

[19] D. Schubert, L. Angerpointner, S. Hecker, S. Sentpali, and M. Buss, "Active vibration cancellation using a multi-harmonic controller," in *Proc. IEEE Conf. Control Technol. Appl.*, 2020, pp. 492–497.

[20] H. Kim, H. Shim, and N. H. Jo, "Adaptive add-on output regulator for rejection of sinusoidal disturbances and application to optical disc drives," *IEEE Trans. Ind. Electron.*, vol. 61, no. 10, pp. 5490–5499, Oct. 2014.

[21] A. Sacks, M. Bodson, and P. Khosla, "Experimental results of adaptive periodic disturbance cancellation in a high performance magnetic disk drive," in *Proc. Amer. Control Conf.*, 1993, pp. 686–690.

[22] S.-C. Wu and M. Tomizuka, "Repeatable runout compensation for hard disk drives using adaptive feedforward cancellation," in *Proc. Amer. Control Conf.*, pp. 382–387, 2006.

[23] P. Zech, D. Plöger, and S. Rinderknecht, "Active control of planetary gearbox vibration using phase-exact and narrowband simultaneous equations adaptation without explicitly identified secondary path models," *Mech. Syst. Signal Process.*, vol. 120, pp. 234–251, Apr. 2019.

[24] Y. H. Guan, W. S. Shepard, T. C. Lim, and M. Li, "Experimental analysis of an active vibration control system for gearboxes," *Smart Mater. Struct.*, vol. 13, no. 5, 2004, Art. no. 1230.

[25] Y. H. Guan, T. C. Lim, and W. S. Shepard, "Experimental study on active vibration control of a gearbox system," *J. Sound Vib.*, vol. 282, no. 3–5, pp. 713–733, 2005.

[26] G. A. R. Fuentes, J. A. Cortés-Romero, Z. Zou, R. Costa-Castelló, and K. Zhou, "Power active filter control based on a resonant disturbance observer," *IET Power Electron.*, vol. 8, no. 4, pp. 554–564, 2015.

[27] F. D. Freijedo, J. Doval-Gandoy, P. Lopez Fernandez-Comesana, and C. Martinez-Penalver, "A signal-processing adaptive algorithm for selective current harmonic cancellation in active power filters," *IEEE Trans. Ind. Electron.*, vol. 56, no. 8, pp. 2829–2840, Aug. 2009.

[28] W. Jung, Y. J. Jang, S. Lim, and S. Won, "Active vibration and flatness control of a strip in a continuous galvanizing line using positive position feedback control," *ISIJ Int.*, vol. 53, no. 5, pp. 854–865, 2013.

[29] M. Saxinger, L. Marko, A. Steinböck, and A. Kugi, "Active rejection control for unknown harmonic disturbances of the transverse deflection of steel strips with control input, system output, sensor output, and disturbance input at different positions," *Mechatronics*, vol. 56, pp. 73–86, 2018. [Online]. Available: https://www.sciencedirect.com/science/article/pii/S0957415818301661

[30] Y. Xu, M. de Mathelin, and D. Knittel, "Adaptive rejection of quasi-periodic tension disturbances in the unwinding of a non-circular roll," in *Proc. Amer. Control Conf.*, 2002, pp. 4009–4014.

[31] L. Marko, M. Saxinger, A. Steinböck, W. Kemmetmüller, and A. Kugi, "Frequency-adaptive cancellation of harmonic disturbances at non-measurable positions of steel strips," *Mechatronics*, vol. 71, 2020, Art. no. 102423, [Online]. Available: https://www.sciencedirect.com/science/article/pii/S0957415820300970

[32] S. M. Kuo and D. R. Morgan, *Active Noise Control Systems*. New York, NY, USA: Wiley, 1996.

[33] E. Bjarnason, "Analysis of the filtered-X LMS algorithm," *IEEE Trans. Speech Audio Process.*, vol. 3, no. 6, pp. 504–514, Nov. 1995.

[34] F. Yang, Y. Cao, M. Wu, F. Albu, and J. Yang, "Frequency-domain filtered-x LMS algorithms for active noise control: A review and new insights," *Appl. Sci.*, vol. 8, 2018, Art. no. 2313.

[35] S. Haykin, *Adaptive Filter Theory*. Englewood Cliffs, NJ, USA: Prentice-Hall, 2001.

[36] I. D. Landau, A. Constantinescu, and D. Rey, "Adaptive narrow band disturbance rejection applied to an active suspension-an internal model principle approach," *Automatica*, vol. 41, no. 4, pp. 563–574, 2005.
[37] B. A. Francis and W. M. Wonham, "The internal model principle of control theory," *Automatica*, vol. 12, no. 5, pp. 457–465, 1976.
[38] H. Su, G.-Y. Tang, and H. Ma, "Damping control for systems with sinusoidal disturbances based on internal model principle," in *Proc. IEEE 27th Int. Symp. Ind. Electron.*, 2018, pp. 206–211.
[39] S. Pigg and M. Bodson, "Adaptive algorithms for the rejection of sinusoidal disturbances acting on unknown plants," *IEEE Trans. Control Syst. Technol.*, vol. 18, no. 4, pp. 822–836, Jul. 2009.
[40] P. Zech, V. Lato, and S. Rinderknecht, "Direct adaptive feedforward compensation of narrowband disturbances without explicit identification of the secondary path model," *J. Sound Vib.*, vol. 401, pp. 282–296, 2017. [Online]. Available: https://www.sciencedirect.com/science/article/pii/S0022460X17303735
[41] G. Pin, "A direct approach for the frequency-adaptive feedforward cancellation of harmonic disturbances," *IEEE Trans. Signal Process.*, vol. 58, no. 7, pp. 3523–3530, Jul. 2010.
[42] D. Patt, L. Liu, J. Chandrasekar, D. S. Bernstein, and P. P. Friedmann, "Higher-harmonic-control algorithm for helicopter vibration reduction revisited," *J. Guidance, Control, Dyn.*, vol. 28, no. 5, pp. 918–930, 2005.
[43] R. Isermann and M. Münchhof, *Identification of Dynamic Systems: An Introduction with Applications*. Berlin, Germany: Springer-Verlag, 2011.
[44] DATAFLEX torque measuring shaft type 42/1000, KTR-Group, 2017. [Online]. Available: https://www.ktr.com/fileadmin/ktr/media/Manuals/49016en000000.pdf

ANIAN BROSCH received the bachelor's and master's degrees in mechanical engineering from the Munich University of Applied Sciences, Munich, Germany, in 2016 and 2018, respectively. Since then, he has been a Research Associate with the Department of Power Electronics and Electrical Drives, Paderborn University, Paderborn, Germany. His research interests include identification and control of electrical drives, in particular model predictive control of highly utilized permanent magnet synchronous motors.

JOHANN RAUHAUS received the bachelor's degree in mechanical engineering from the OWL University of Applied Sciences and Arts, Lemgo, Germany, in 2016, and the master's degree in mechanical engineering from Paderborn University, Paderborn, Germany, in 2019. Since 2019, he has been a Research Fellow with the Chair of Design and Drive Technology, Paderborn University. His research interests include multi motor drive systems and electromechanical actuators for brake systems.

OLIVER WALLSCHEID (Member, IEEE) received the bachelor's and master's degrees (Hons.) in industrial engineering and the doctorate degree (Hons.) in electrical engineering from Paderborn University, Paderborn, Germany, in 2010, 2012, and 2017, respectively. Since then, he has been a Senior Research Fellow with the Department of Power Electronics and Electrical Drives, Paderborn University. He is currently an Acting Professor with the Department of Automatic Control, Paderborn University. His research interests data-driven identification and intelligent control of electrical power systems in decentralized grids, power electronics, and drives.

DETMAR ZIMMER studied mechanical engineering from the University of Stuttgart, Stuttgart, Germany, where he received the Dipl.-Ing. and Dr.-Ing. degrees in 1984 and 1990, respectively. He is currently a Professor and the Head of the Chair of Design and Drive Technology with Paderborn University, Paderborn, Germany. Afterwards, he was with Lenze SE for 11 years, last responsible for the Geared Motors Department. In 2001, he was appointed to the current Professorship. He is a member of the Scientific Society of Product Development WiGeP and an Associate Editor for the journal *Konstruktion*. His research interests include electromechanical drives, additive manufacturing, and combining both disciplines.

JOACHIM BÖCKER (Senior Member, IEEE) studied electrical engineering from the Berlin University of Technology, Berlin, Germany, where he received the Dipl.-Ing. and Dr.-Ing. degrees in 1982 and 1988, respectively. He is currently a Professor and the Head of the Department of Power Electronics and Electrical Drives, Paderborn University, Paderborn, Germany. From 1988 to 2001, he was with AEG and Daimler Research as the Head of the Control Engineering Team, Electrical Drive Systems Laboratory. In 2001, he started his own business in the area of control engineering, electrical drives and power electronics. In 2003, he was appointed to the current professorship. His research interests include electrical drives, particularly for EVs and HEVs, energy management strategies for vehicles and smart grids, and converters for power supplies, EV chargers, and renewables.